

# Micro-structural and Biaxial Creep Properties of the Swine Uterosacral–Cardinal Ligament Complex

TING TAN,<sup>1</sup> NATHAN M. CHOLEWA,<sup>2</sup> SCOTT W. CASE,<sup>2</sup> and RAFFAELLA DE VITA<sup>1</sup>

<sup>1</sup>Mechanics of Soft Biological Systems Laboratory, Department of Biomedical Engineering and Mechanics, Virginia Tech, Blacksburg, VA 24061, USA; and <sup>2</sup>Materials Response Group, Department of Biomedical Engineering and Mechanics, Virginia Tech, Blacksburg, VA 24061, USA

(Received 19 February 2016; accepted 20 May 2016; published online 2 June 2016)

Associate Editor Ender A. Finol oversaw the review of this article.

**Abstract**—The uterosacral ligament and cardinal ligament (USL/CL) complex is the major suspensory tissue of the uterus, cervix, and vagina. This tissue is subjected primarily to bi-axial forces *in-vivo* that significantly alter its structure and dimension over time, compromising its support function and leading to pelvic floor disorders. In this study, we present the first rigorous characterization of the collagen fiber microstructure and creep properties of the swine USL/CL complex by using scanning electron microscopy and planar biaxial testing in combination with three-dimensional digital image correlation. Collagen fiber bundles were found to be arranged into layers. Although the fiber bundles were oriented in multiple directions, 80.8% of them were aligned within  $\pm 45^\circ$  to the main *in-vivo* loading direction. The straightness parameter, defined as the ratio of the end-to-end distance of a fiber bundle to its length, varied from 0.28 to 1.00, with 95.2% fiber bundles having a straightness parameter between 0.60 and 1.00. Under constant equi-biaxial loads of 2 and 4 N, the USL/CL complex exhibited significant creep both along the main *in-vivo* loading direction (the parallel direction) and along the direction perpendicular to it (the perpendicular direction). Specifically, over a 120-min period, the mean strain increased by 20–34% in the parallel direction and 33–41% in the perpendicular direction. However, there was no statistically significant difference in creep strains observed after 120 min between the parallel and perpendicular directions for either the 2 or 4 N load case. Creep proceeded slightly faster in the perpendicular direction under the equi-biaxial load of 2 N than under the equi-biaxial load of 4 N ( $p = 0.3696$ ). It proceeded significantly faster in the parallel direction under the equi-biaxial loads of 2 N than under the equi-biaxial loads of 4 N ( $p = 0.0284$ ). Overall, our findings contribute to a greater understanding of the biomechanical

properties of the USL/CL complex that is needed for the development of new surgical reconstruction methods and mesh materials for pelvic floor disorders.

**Keywords**—Pelvic floor connective tissue, Uterosacral ligament, Cardinal ligament, Scanning electron microscopy, Creep, Planar biaxial test, Digital image correlation.

## INTRODUCTION

Every year millions of women are affected by pelvic floor disorders (PFDs) such as urinary incontinence, fecal incontinence, and pelvic organ prolapse. In the United States, the number of women with at least one PFD is projected to significantly increase from 28.1 millions in 2010 to 43.8 millions in 2050 with 55, 59, and 46% increases in urinary incontinence, fecal incontinence, and pelvic organ prolapse, respectively.<sup>42</sup> The lifetime risk of surgery for PFDs is 11.1% with a 29.2% risk of an additional surgery.<sup>23</sup> The annual direct cost for pelvic organ prolapse surgeries alone is approximately one billion dollars.<sup>36</sup> Thus, given the projected increase in the number of affected women, PFDs are expected to place a significant burden on the quality of life of women and a financial strain on the health care system.

Pelvic floor muscles, fasciae, and ligaments are the main supportive structures of the pelvic organs. They maintain the organs in their anatomical positions allowing them to perform their normal physiological function. These supportive structures can be weakened or damaged by labor, delivery, menopause, aging, and obesity, leading to the development of PFDs.<sup>10,17,22</sup> The USL and CL are apical supportive structures of the vagina, cervix, and uterus. They are bilateral visceral ligaments connected together distally at the cervix

Address correspondence to Raffaella De Vita, Mechanics of Soft Biological Systems Laboratory, Department of Biomedical Engineering and Mechanics, Virginia Tech, Blacksburg, VA 24061, USA. Electronic mail: tt95@vt.edu, ncholewa@vt.edu, scase@vt.edu, devita@vt.edu

and/or upper vagina without a clear boundary between them (see Fig. 1a) and attach the organs proximally to the sacrum and laterally to the pelvic sidewalls, respectively.<sup>26</sup> They are often referred to as the USL/CL complex. When the supportive function of this complex is compromised, a uterine or vaginal prolapse may develop.<sup>7</sup> The USL and CL not only play a pivotal role in supporting the uterus, cervix, and vagina in healthy women but they also are extensively used as anchor structures in surgical procedures for pelvic organ prolapse.<sup>2,12,14,31</sup> During these surgeries, the ligaments are often stretched and tensed in an *ad-hoc* manner. However, the amount of stretch and tension placed on them can seriously compromise the successful outcome of the surgeries. For instance, one study attributed post hysterectomy vaginal vault prolapse to excessive tension placed on these ligaments during surgery.<sup>12</sup> Artificial mesh materials have been also used in surgeries for PFDs. The mesh products are expected to have appropriate biomechanical properties,<sup>4,18</sup> similar to those of healthy and strong suspensory tissues.<sup>13</sup> Therefore, investigating the mechanical properties of the USL/CL complex is critical for the development of new surgical reconstruction strategies and mesh materials for PFDs.

The mechanical properties of the USL and CL have only recently been investigated. Uniaxial force-displacement data have been obtained by performing tensile tests on *ex-vivo* specimens from patients undergoing hysterectomy<sup>27</sup> and by conducting tensile and stress-relaxation tests on *in-vivo* specimens from women affected by pelvic organ prolapse.<sup>16,32</sup> Uniaxial force-displacement data were also collected on *ex-vivo* rat specimens from the vagina-ligament complex by means of tensile tests.<sup>21</sup> Although force-displacement data provide useful information on the mechanical behavior of the USL and CL, they are highly dependent on the dimensions of the tested specimens. Mechanical properties of these ligaments that are independent of the dimensions of the tested specimens have been determined from stress-strain data.<sup>3,19,29,37,41</sup> The mean strength and tensile modulus of the USL were reported for *ex-vivo* specimens from monkeys,<sup>41</sup> female cadavers,<sup>19,29</sup> and swine.<sup>37</sup> The strain-dependent tensile modulus of the USL was found to increase in post menopausal monkeys due to hormone replacement therapy.<sup>41</sup> The USL of nulliparous women was reported to have lower stiffness and strength than the USL of parous women.<sup>19</sup> Compared to the round and the broad ligaments, the USL was found to have higher tangent modulus at both low and high strain levels.<sup>29</sup> The tensile properties of the USL/CL specimens were highly dependent on their location relative to the uterus, cervix, and vagina in the swine.<sup>37</sup> Recently, our group has characterized

the elastic and stress relaxation properties of these ligaments by performing planar biaxial tests.<sup>3</sup> The swine USL/CL complex was found to be stiffer along the main physiological loading direction but relaxed equally under equi-biaxial strain along such direction and the direction perpendicular to it, with higher relaxation occurring at lower strain.

*In-vivo*, the USL/CL complex is subjected to multi-axial loads that are, for example, imposed by the weight of the pelvic organs. The deformation over time under constant loads, the so-called creep behavior, has not been characterized for these ligaments despite its physiological relevance. Creep has been studied for other biological soft tissues such as rat and rabbit medial collateral ligaments,<sup>11,24,38–40</sup> porcine mitral and aortic valves,<sup>1,8,35</sup> and human amnion<sup>20</sup> to name but a few. It was found that the creep strain and creep rate in rat medial collateral ligaments were highly dependent on the magnitude of the applied stress.<sup>11,24</sup> In the rabbit medial collateral ligaments, creep was attributed to the straightening of collagen fibers under low stress and damage of such fibers at high stress.<sup>40</sup> The decrease in creep rate with the increase in stress was explained by fewer collagen fibers left to be recruited during creep as the stress increased.<sup>38,40</sup> Creep in the aortic valve was found to be stress dependent and differed in the circumferential and radial directions.<sup>1</sup> In the human amnion, creep measured *via* uniaxial tests was significantly larger than creep measured *via* inflation tests at a comparable tension.<sup>20</sup> To date, the only planar biaxial creep studies on biological soft tissues have been conducted by Grashow *et al.*<sup>8</sup> and Stella *et al.*<sup>35</sup> However, these authors reported negligible biaxial creep for mitral valves<sup>8</sup> and aortic valves.<sup>35</sup>

In this study, we investigate the micro-structural and mechanical properties of the USL/CL complex using the swine as animal model. Previous studies suggested that swine is a suitable animal model for pelvic floor research<sup>5</sup> and, more specifically, the histological and mechanical properties of the USL/CL complex are very similar to those in humans.<sup>9,37</sup> By using scanning electron microscopy (SEM), we reveal the organization of collagen fibers, which represent the main structural components of these ligaments. More specifically, we quantify the straightness and the alignment of collagen fiber bundles. We determine the biaxial creep properties of the swine USL/CL complex by using a planar biaxial testing system in conjunction with the Digital Image Correlation (DIC) method. This method provides more accurate strain measurements than previously used techniques such as those relying on gauge length measurements<sup>19,29,41</sup> or on optically tracking a few markers.<sup>3,37</sup> The DIC method is employed here to measure the deformation over time experienced by the USL/CL complex under constant

equi-biaxial loads. Overall, this study advances our limited knowledge about the micro-structural and mechanical properties of some components of the pelvic connective tissues that play a crucial role in the surgical treatment of PFDs.

## MATERIAL AND METHODS

### *Specimen Preparation*

This study was conducted with the approval of the Institutional Animal Care and Use Committee (IACUC) at Virginia Tech. Seven adult domestic swine were obtained from a slaughterhouse. The swine were 3 to 4 years old and had masses of approximately 200 kg. The harvesting technique for USL/CL complex was described in detail in our previous study.<sup>37</sup> The ligaments were carefully dissected, hydrated in phosphate-buffered saline solution (PBS, pH 7.4, Fisher Scientific, USA) and then frozen at  $-20^{\circ}\text{C}$ .<sup>30</sup> They were thawed at room temperature before being used for SEM or creep tests.

### *SEM Examination*

Six square-shaped specimens were collected from three USL/CL complexes. More precisely, each specimen was isolated from the USL and CL as shown in Fig. 1a and cut so that the sides were parallel and perpendicular to the main *in-vivo* loading direction. Hereafter, the direction that is parallel to the main *in-vivo* loading direction of the ligaments will be termed the parallel direction and the direction that is perpendicular to it will be termed the perpendicular direction. The specimen was then fixed overnight in 10% buffered formalin, washed in phosphate-buffered saline solution (PBS, pH 7.4, Fisher Scientific, USA), post-fixed in

osmium tetroxide, and dried in a critical point dryer (Model 28000, LADD Research Industries, Williston, Vermont, USA). It was then immersed in liquid nitrogen and fractured with a sharp razor blade in order to reveal three different sections: one planar section (section 1 in Fig. 1b) and two through-thickness sections (sections 2 and 3 in Fig. 1b). After being sputter coated with gold, these sections were examined using an SEM (EVO 40, Carl Zeiss, Jena, Germany) at  $1,000\times$  and  $20,000\times$  magnifications.

Twenty-one SEM images from section 1 (Fig. 1b) of six specimens at  $1,000\times$  magnification were analyzed to measure collagen fiber bundle straightness and global orientation angle relative to the parallel direction. Fiber bundles on these images were traced and their length and end point coordinates were determined using NeuronJ,<sup>28</sup> a plugin of the ImageJ software (v1.48, NIH, Bethesda, MA, USA). A total of 336 fiber bundles were detected. From the coordinates of the end points, the end-to-end distance,  $L_0^{(i)}$ , of the  $i$ th fiber bundle and the global orientation angle,  $\theta^{(i)}$ , with respect to the parallel direction were calculated (Fig. 2). The straightness parameter of the  $i$ -th fiber bundle was defined as  $L_0^{(i)}/L_f^{(i)}$  where  $L_f^{(i)}$  is the length of  $i$ th fiber bundle (Fig. 2). The mean thickness,  $t^{(i)}$ , was computed by averaging the thickness measurements from three randomly chosen locations along the length of the fiber bundle using ImageJ. The area of the  $i$ th fiber bundle,  $S^{(i)}$ , was then calculated as the product of its length  $L_f^{(i)}$  and mean thickness  $t^{(i)}$ . The fraction,  $f^{(i,j)}$ , of fiber bundles with a given straightness parameter  $L_0^{(i)}/L_f^{(i)}$  and global orientation angle  $\theta^{(i)}$  was computed as  $f^{(i,j)} = \Sigma_{k=1}^m S^{(k)} / \Sigma_{k=1}^n S^{(k)}$ , where  $m$  denotes the number of fiber bundles with straightness parameter  $L_0^{(i)}/L_f^{(i)}$  and global orientation angle  $\theta^{(i)}$ .

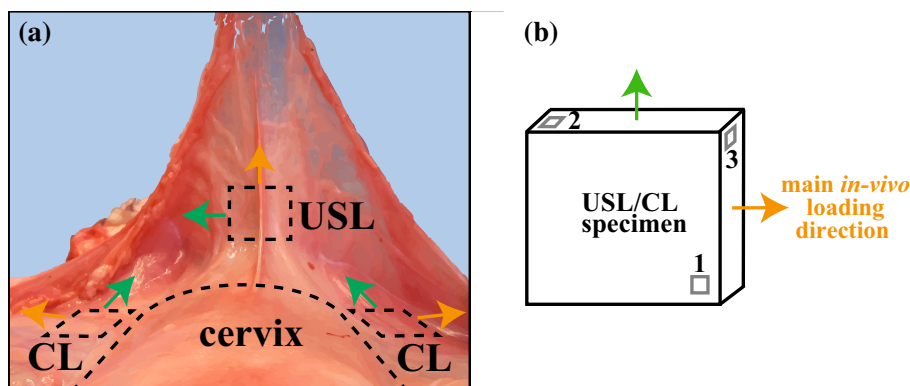


**FIGURE 1.** (a) Picture of the swine USL/CL complex and its attachment to the cervix (transverse plane view). (b) Locations of the USL/CL specimen sections used for SEM analysis. The main *in-vivo* loading direction of the ligaments is denoted using an orange arrow and the direction that is perpendicular to this is denoted using a green arrow. These directions are referred to as the parallel and perpendicular directions, respectively.

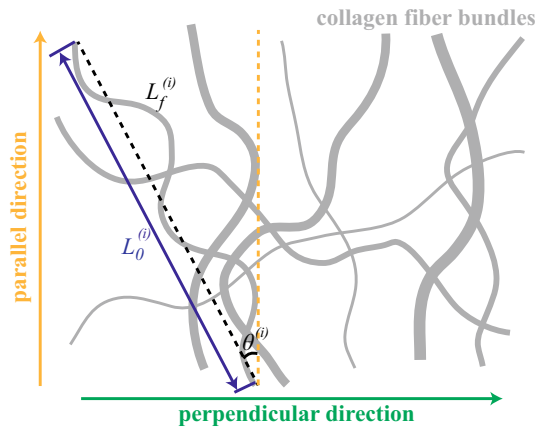


**FIGURE 2.** Measured parameters: fiber bundle length  $L_f^{(i)}$ , end-to-end fiber bundle distance  $L_0^{(i)}$ , and global fiber orientation angle  $\theta^{(i)}$  computed with respect to the parallel direction.

and  $n = 336$  denotes the total number of fiber bundles detected in the twenty-one SEM images that were analyzed. The fraction of fiber bundles with different straightness parameters was computed as  $g^{(i)} = \sum_{k=1}^p S^{(k)} / \sum_{k=1}^n S^{(k)}$ , where  $p$  denotes the number of fiber bundles with straightness parameter  $L_0^{(i)} / L_f^{(i)}$ . The fraction of fiber bundles with different global orientation angles with respect to the parallel direction was computed as  $h^{(j)} = \sum_{k=1}^q S^{(k)} / \sum_{k=1}^n S^{(k)}$ , where  $q$  denotes the number of fiber bundles with global orientation angle  $\theta^{(j)}$ .

### Biaxial Creep Testing

Specimens ( $n = 25$ ) from four sows were cut into squares having side of length 3 cm parallel and perpendicular to the main *in-vivo* loading direction. The thickness of each specimen was measured by means of a digital caliper (accuracy  $\pm 0.05$  mm, Series 573, Mitutoyo, Japan) under a 50 g compressive load. For mechanical testing, each specimen was then immersed in methylene blue, 1% aqueous solution (Fisher Science Education, USA), and gripped by four safety pins on each side. A high-contrast speckle pattern was then created on the surface of the specimen with aerosol fast dry gloss white paint (McMaster-Carr, USA).<sup>15</sup> Two CCD cameras (Prosilica GX 1660, Allied Vision Technologies, Exton, Pennsylvania, USA) equipped with macro lenses (AT-X 100mm F2.8 AT-X M100 Pro D Macro Lens, Tokina, Tokyo, Japan) were employed to capture high resolution ( $1600 \times 1200$  pixel) images of a  $12 \text{ mm} \times 9 \text{ mm}$  plastic grid with 4 mm spacing. These images were used to calibrate a 3-D DIC (VIC-3D, Correlated Solutions, Columbia, South Carolina, USA) for non-contact strain measurement.

After calibration, the safety pins on each side of the specimen were connected to four pulleys attached to four actuators (accuracy:  $5 \mu\text{m}$ ) of a planar biaxial testing system (Instron, UK). Each specimen was oriented so that its main *in-vivo* loading direction (the parallel direction) and the direction perpendicular to it (the perpendicular direction) were aligned with the two loading axes of the biaxial testing system. The capacity of the four load cells of the planar biaxial testing system was 20 N (accuracy: 0.02 N). The specimen was then immersed into an enclosed bath made of acrylic glass (Perspex, UK) that was fully filled with PBS at room temperature ( $21^\circ\text{C}$ ). Starting from zero displacement, the specimen was preloaded to 0.1 N and preconditioned from 0.1 to 0.6 N at 0.1 mm/s displacement rate for 10 cycles. Following preconditioning, the specimen was unloaded and allowed to recover for 10 min. Each specimen was then stretched at 0.1 mm/s displacement rate until equi-biaxial loads of 2 N ( $n = 15$  specimens) or 4 N ( $n = 10$  specimens) were detected. These equi-biaxial loads were kept constant for 120 min. The full field displacement and Lagrangian strain were determined by postprocessing the specimen images obtained during equi-biaxial tests using the VIC-3D software (v7, VIC-3D, Correlated Solutions, Columbia, SC, USA) after these images underwent background subtraction for the presence of the bath plastic cover and PBS. We note that additional specimens were subjected to equibiaxial loads of 4 N. However, these specimens failed at the grips and thus the data collected from these samples were excluded from this study.

For each specimen, nominal axial stresses in the parallel and perpendicular directions were calculated by dividing the axial loads in the corresponding directions by the specimen undeformed cross-sectional areas. The specimen cross-sectional area was assumed to be rectangular. Lagrangian axial strains in the parallel and perpendicular directions were computed by averaging the local Lagrangian axial strains in the corresponding directions computed over a  $1 \text{ cm} \times 1 \text{ cm}$  central region of the specimen using the 3D-DIC methods (Fig. 3). Normalized Lagrangian axial strains in the parallel and perpendicular directions were determined by dividing the Lagrangian axial strains by the initial Lagrangian axial strain (i.e., the Lagrangian axial strain at beginning of the creep test) in the corresponding directions. Hereafter and throughout this manuscript, *stress* will be used to denote nominal axial stress, *strain* to denote Lagrangian axial strain, and *normalized strain* to denote normalized Lagrangian axial strain. For each tested specimen, creep rates in the parallel or perpendicular direction were computed as the slopes of the linear regression lines of the normalized strain data in the corresponding parallel or

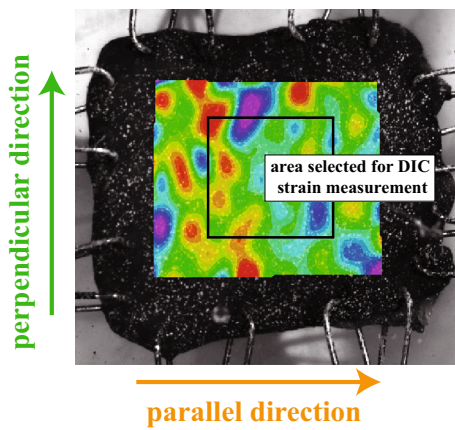


**FIGURE 3.** Area selected on the specimen surface for the measurement of local Lagrangian axial strains *via* the DIC method. Shown here is the strain map in the parallel direction for one specimen.

perpendicular direction vs. time data using logarithmic scales.<sup>11</sup>

#### Statistical Analysis

Means and standard deviations were calculated for the axial loads and corresponding stresses, initial strains (i.e., strain at the beginning of the creep tests), and normalized strains over time in both parallel and perpendicular directions for two groups of specimens: one group of  $n = 15$  specimens subjected to equi-biaxial loads of 2 N and one group of  $n = 10$  specimens subjected to equi-biaxial loads of 4 N. The Student's  $t$  test was used to compare the means of the normalized strain at 120 min and the creep rate between the parallel and perpendicular directions and between equi-biaxial loads of 2 and 4 N. The threshold chosen for statistical significance was 0.05. Data were analyzed using the JMP statistical software (JMP 10, SAS Institute Inc.).

## RESULTS

### SEM Examination

Representative scanning electron micrographs of the USL/CL complex are shown in Fig. 4. Most collagen fibers were oriented along the main *in-vivo* loading direction of the ligaments, the parallel direction. However, some fibers were oriented at small angles off such direction (Figs. 4a–4d). The collagen fibers were found to be arranged into layers (Figs. 4e and 4f). Some layers contained more collagen fibers than others and, in these layers, the collagen fibers were organized into bundles (Fig. 4f). The collagen fiber bundles (Figs. 4a and 4c) and

collagen fibers (Figs. 4b and 4d) were observed to have different straightness levels.

The fractions of fiber bundles with different straightness parameters and global orientation angles relative to the parallel direction are presented in a three-dimensional bar plot in Fig. 5. Each fiber bundle with its own straightness parameter and global orientation angle was considered to generate this plot. The fiber bundles were spread everywhere within the ligament, as expected, and the straightness parameter varied from 0.28 to 1.00. Most of the fiber bundles were aligned at a small angle off the parallel direction and most of them had a relatively high straightness parameter indicating low fiber bundle crimping. The average straightness parameter of fiber bundles that were mainly aligned along the parallel direction, between  $-10^\circ$  and  $10^\circ$ , was 0.854. This was very similar to the average straightness parameter of fiber bundles mainly aligned along the perpendicular direction, between  $+80^\circ$  and  $+90^\circ$  and between  $-90^\circ$  and  $-80^\circ$ , which was 0.830. The fractions of fiber bundles with different straightness parameters (regardless of the fiber bundle global orientation angles) are shown in the histogram in Fig. 6. The empirical data revealed a skewed right distribution spreading from 0.28 to 1.00, with 95.2% fiber bundles having a straightness parameter between 0.60 and 1.00. The highest fraction of collagen fiber bundles, which was 15%, had a straightness parameter between 0.90 and 0.92. The histogram of fiber bundle orientation angles (regardless of the fiber bundle straightness parameters) is presented in Fig. 7. It can be seen that 80.8% fiber bundles had a global orientation angle between  $-45^\circ$  and  $+45^\circ$ , while 19.2% fiber bundles had a global orientation angle between  $+45^\circ$  and  $+90^\circ$  and between  $-90^\circ$  and  $-45^\circ$ .

### Biaxial Creep

The axial loads, corresponding stresses, and initial strains (mean  $\pm$  standard deviation) used during the creep tests at constant equi-biaxial loads of 2 and 4 N are reported in Tables 1 and 2, respectively. For both loads, the mean stresses in the parallel and perpendicular directions were nearly identical, while the mean initial strain measured in the perpendicular direction was always larger than the mean initial strain in the parallel direction (Tables 1 and 2). We note that mean initial strains for the equi-biaxial loads of 2 N are 0.116 and 0.152 in the parallel and perpendicular directions, respectively, and that the mean initial strains for the equi-biaxial loads of 4 N are 0.216 and 0.263 in the parallel and perpendicular directions, respectively. The mean and standard deviation of the normalized strain data vs. time obtained from creep tests at constant

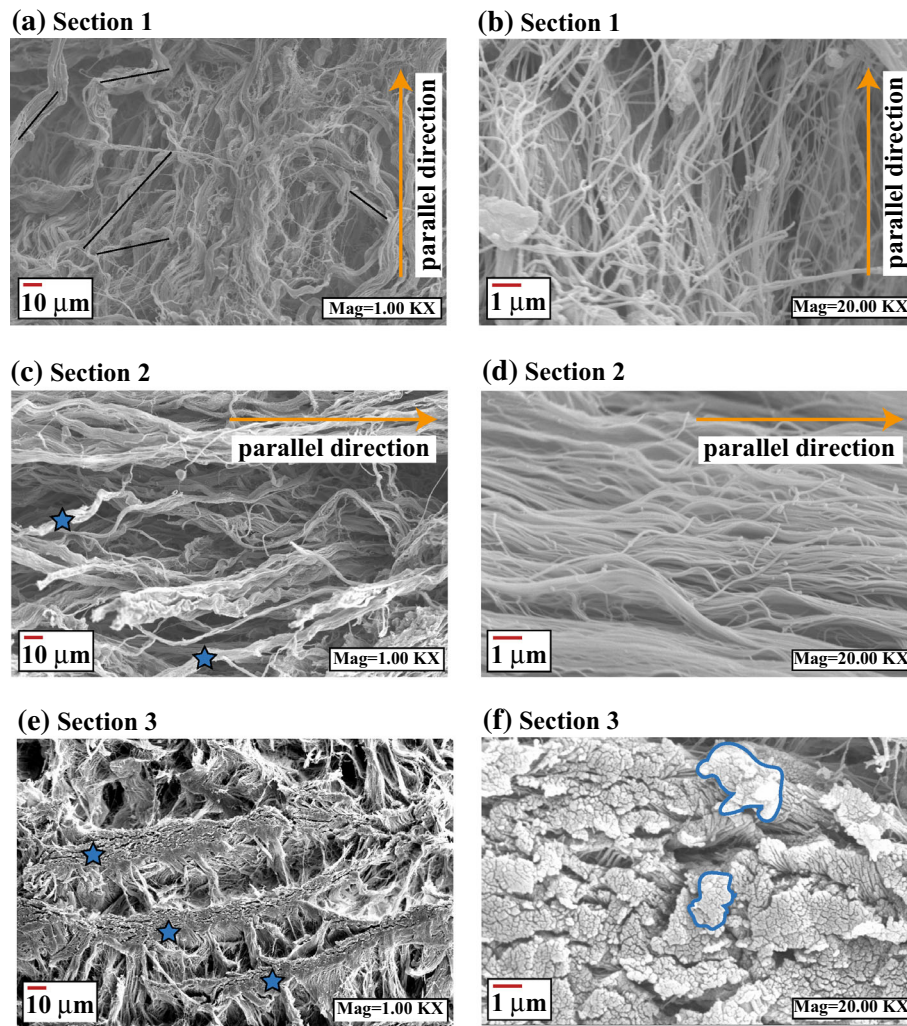


**FIGURE 4.** (a), (b) SEM of the in-plane specimen cross-section (section 1 in Fig. 1) at 1,000 $\times$  and 20,000 $\times$  magnifications, respectively. In (a) the black lines indicate the directions of collagen fiber bundles. (c), (d) SEM of the out-of-plane specimen cross-section (section 2 in Fig. 1) at 1,000 $\times$  and 20,000 $\times$  magnifications, respectively. In (c) the star symbols denote the collagen fiber bundles. The main *in-vivo* loading direction of the ligaments, the parallel direction, is denoted using an arrow in (a)–(d). (e), (f) SEM of the out-of-plane specimen cross-section (section 3 in Fig. 1) at 1,000 $\times$  and 20,000 $\times$  magnifications, respectively. In (e) the star symbols denote three layers of collagen fibers and in (f) the contour lines denote the cross-sections of collagen fiber bundles.

equi-biaxial loads of 2 and 4 N are presented in Fig. 8. Despite the large variation, the creep of all the specimens in both loading directions had a similar trend over the 120 min duration of the tests: the normalized strain increased quickly over the first 18 min and very slowly over the last 35 min (Fig. 8). At the constant equi-biaxial load of 2 N, the creep at 18 min (the difference between the mean normalized strain at 18 min and the mean normalized strain at 0 min) was approximately 64 and 71% of the creep at 120 min (the difference between the mean normalized strain at 120 min and the mean normalized strain at 0 min) in the parallel and perpendicular directions, respectively (Fig. 8a). At the constant equi-biaxial load of 4 N, the creep at 18 min was approximately 50 and 77% of the creep measured at 120 min in the parallel and

perpendicular directions, respectively (Fig. 8b). The mean normalized strain of the ligaments over time appeared to be different in the two loading directions.

The mean and standard deviation of the normalized strain data at 120 min in the parallel and perpendicular directions computed from creep tests at constant equi-biaxial loads of 2 and 4 N are shown in Fig. 4. The mean strain at 120 min from creep tests at constant equi-biaxial loads of 2 N was found to be 1.41 and 1.32 times the initial mean strain in the perpendicular and parallel directions, respectively. The mean strain at 120 min from creep tests at constant equi-biaxial loads of 4 N was found to be 1.30 and 1.20 times the initial mean strain in the perpendicular and parallel directions, respectively. In the perpendicular direction, the mean normalized strain obtained from creep tests at constant

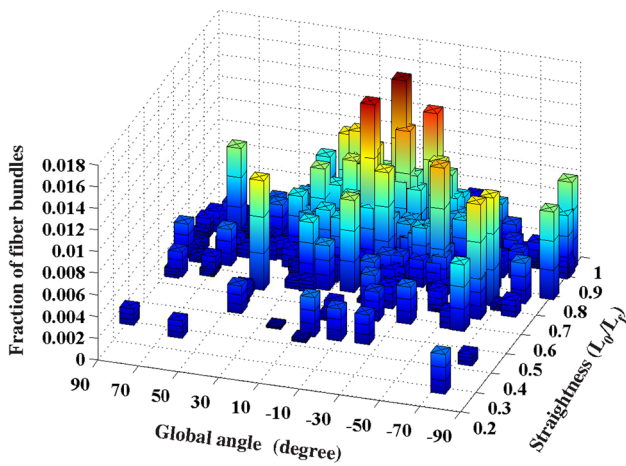


**FIGURE 5.** Fractions of collagen fiber bundles with different straightness parameters and global orientation angles (with respect to the 0° parallel direction). The reported data were obtained by analyzing  $n = 21$  SEM images.

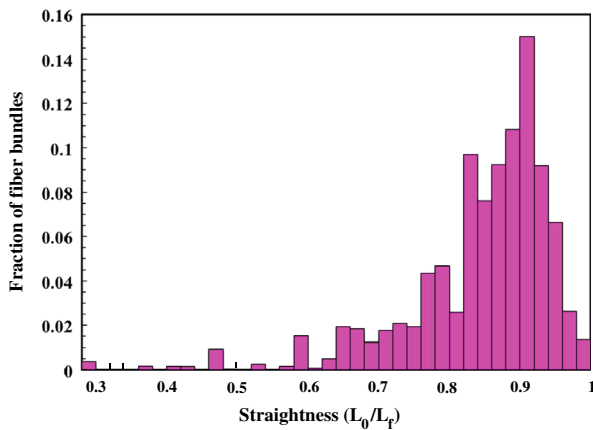


**FIGURE 6.** Fractions of collagen fiber bundles with straightness parameters that differ by 0.02. The reported data were obtained by analyzing  $n = 21$  SEM images.

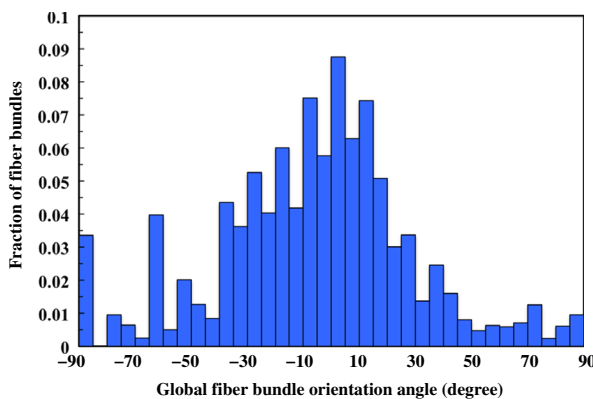


**FIGURE 7.** Fractions of collagen fiber bundles with global orientation angles with respect to the parallel direction that differ by 5° from -90° to 90°. The reported data were obtained by analyzing  $n = 21$  SEM images.

equi-biaxial loads of 2 N was slightly larger than the mean normalized strain obtained from creep tests at constant equi-biaxial loads of 4 N ( $p = 0.2541$ ). In the parallel direction, the mean normalized strain obtained from creep tests at constant equi-biaxial loads of 2 N was much larger, but still not significantly larger, than the mean normalized strain obtained from creep tests at constant equi-biaxial loads of 4 N ( $p = 0.0662$ ). In other words, the ligaments experienced more creep under constant equi-biaxial loads of 2 N than under constant equi-biaxial loads of 4 N. By comparing the mean strain values at 120 min, one can observe that the ligaments exhibited more creep in the perpendicular direction than in the parallel direction. However, our statistical analysis showed that, at 120 min, there was no significant difference between the mean normalized strains in the parallel and perpendicular directions for both constant equi-biaxial loads of 2 N ( $p = 0.2690$ ) and 4 N ( $p = 0.0858$ ) (Fig. 9).

The mean and standard deviation of the creep rate at equi-biaxial loads of 2 and 4 N in the parallel and perpendicular directions were also determined (Fig. 10). The mean creep rate at equi-biaxial loads of 2 N was found to be 0.050 and 0.054 in the perpendicular and parallel directions, respectively, while the mean creep rate at equi-biaxial loads of 4 N was found to be 0.041 and 0.031 in the perpendicular and parallel directions, respectively. In the ligaments, creep proceeded significantly faster at equi-biaxial loads of 2 N than at equi-biaxial loads of 4 N in the parallel direction ( $p = 0.0284$ ). It proceeded slightly faster at equi-biaxial loads of 2 N than at equi-biaxial loads of 4 N in the perpendicular direction ( $p = 0.3696$ ). Additionally, no significant difference between the mean creep rate of the ligaments in the parallel and perpendicular directions at both equi-biaxial loads of 2 N ( $p = 0.5709$ ) and 4 N ( $p = 0.3542$ ) was noted.

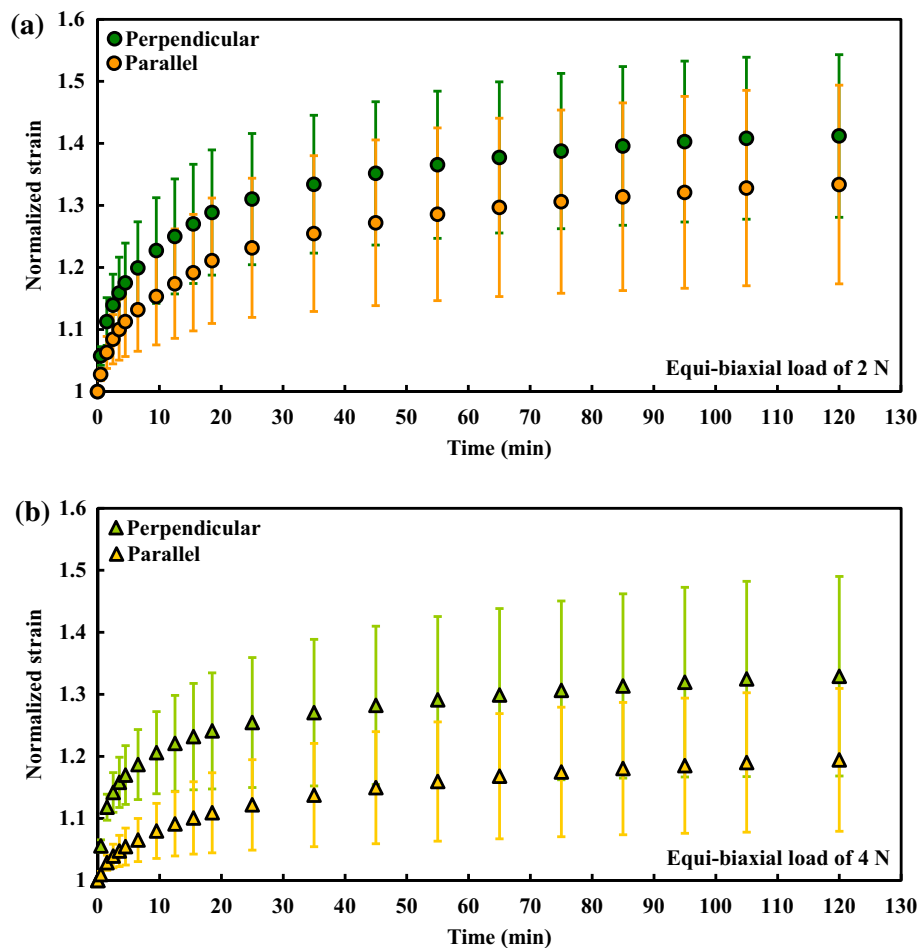
To investigate the effect of stress on the creep behavior of the USL/CL complex, the normalized strain at three chosen time points ( $t = 2.5$ ,  $t = 12.5$ , and  $t = 120$  min) in the parallel and perpendicular directions were analyzed with the corresponding stress (Fig. 11). Two of the three time points were chosen within the first 20 min of the creep tests when a large increase in normalized strain was detected (i.e.,  $t = 2.5$  and 12.5 min), and one time point was selected toward the end of the creep tests ( $t = 120$  min). Linear regression lines for the three time points are plotted with the normalized strain-stress data (Fig. 11). These lines indicate that the ligaments experienced slightly less creep under high stress levels. A more clear decrease in normalized strain with stress can be observed at  $t = 120$  min. The creep rate vs. stress data in the parallel and perpendicular directions are reported in Fig. 12. Large inter-sample variation is observed. This

**TABLE 1.** Creep test parameters for  $n = 15$  specimens (thickness:  $0.691 \pm 0.226$  mm) subjected to constant equi-biaxial loads of 2 N.

Direction	Mechanical quantity	Value (mean $\pm$ SD)
Parallel	Load (N)	$2.09 \pm 0.19$
	Stress (MPa)	$0.153 \pm 0.066$
	Initial strain	$0.116 \pm 0.065$
Perpendicular	Load (N)	$2.00 \pm 0.07$
	Stress (MPa)	$0.142 \pm 0.061$
	Initial strain	$0.152 \pm 0.076$

**TABLE 2.** Creep test parameters for  $n = 10$  specimens (thickness:  $0.652 \pm 0.152$  mm) subjected to constant equi-biaxial loads of 4 N.

Direction	Mechanical quantity	Value (mean $\pm$ SD)
Parallel	Load (N)	$3.87 \pm 0.12$
	Stress (MPa)	$0.284 \pm 0.080$
	Initial strain	$0.216 \pm 0.125$
Perpendicular	Load (N)	$4.02 \pm 0.08$
	Stress (MPa)	$0.289 \pm 0.080$
	Initial strain	$0.263 \pm 0.218$

**FIGURE 8.** Mean and standard deviation of the normalized strain over time in the parallel and perpendicular directions for (a)  $n = 15$  specimens subjected to constant equi-biaxial loads of 2 N and (b) for  $n = 10$  specimens subjected to constant equi-biaxial loads of 4 N.

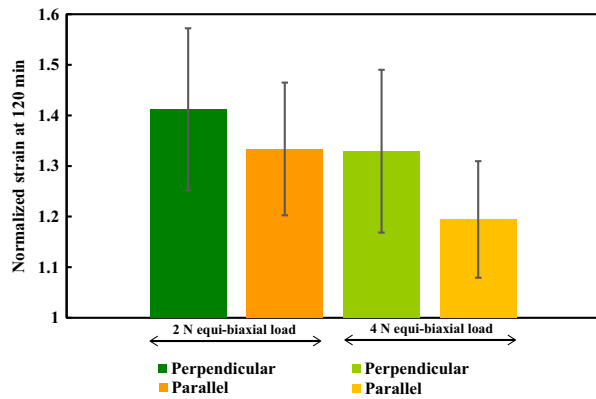


**FIGURE 9.** Mean and standard deviation of normalized strain at  $t = 120$  min for  $n = 15$  specimens subjected to constant equi-biaxial loads of 2 N and for  $n = 10$  specimens subjected to constant equi-biaxial loads of 4 N in the parallel and perpendicular directions. No significant differences between the mean normalized strains in the parallel and perpendicular directions for both constant equi-biaxial loads of 2 N ( $p = 0.2690$ ) and 4 N ( $p = 0.0858$ ). No significant difference between the normalized strains at constant equi-biaxial loads of 2 and 4 N in the perpendicular direction ( $p = 0.2541$ ) and in the parallel direction ( $p = 0.0662$ ).

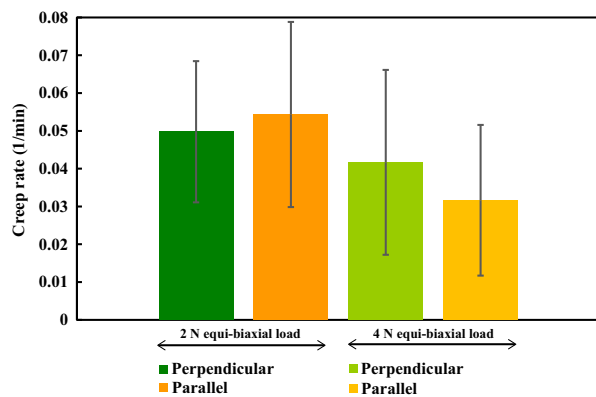


**FIGURE 10.** Mean and standard deviation of creep rate for  $n = 15$  specimens subjected to constant equi-biaxial loads of 2 N and for  $n = 10$  specimens subjected to constant equi-biaxial loads of 4 N in the parallel and perpendicular directions. There was no significant difference between the creep rates in the parallel and perpendicular directions for both constant equi-biaxial loads of 2 N ( $p = 0.5709$ ) and 4 N ( $p = 0.3542$ ) and no significant difference between the creep rates at constant equi-biaxial loads of 2 and 4 N in the perpendicular direction ( $p = 0.3696$ ). There was significant difference between the creep rates at constant equi-biaxial loads of 2 and 4 N in the parallel direction ( $p = 0.0284$ ).

prevents clearly correlating the creep rate and the stress in both loading directions.

## DISCUSSION

Collagen fibers were observed on three different sections of the USL/CL complex using SEM (Fig. 1b). The ligaments were found to be composed of layers of

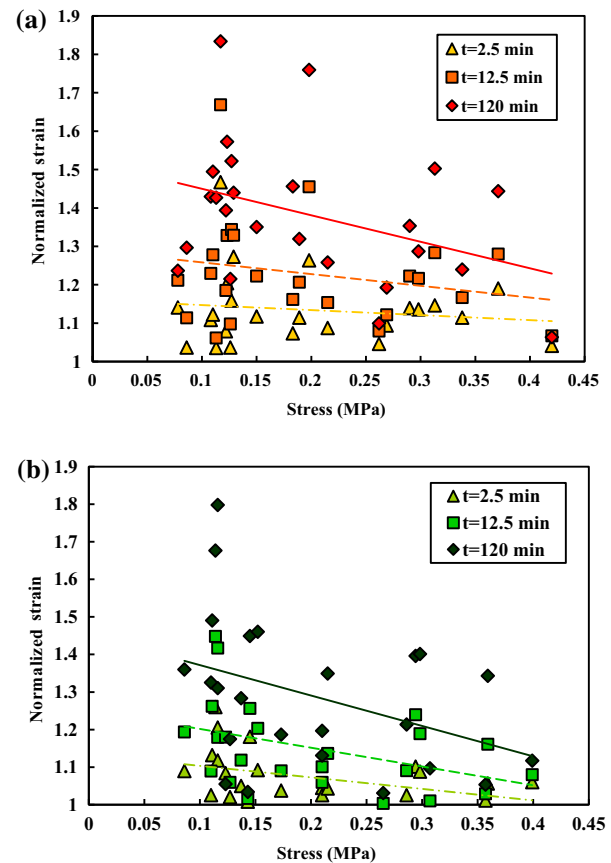


**FIGURE 11.** Normalized strain at  $t = 2.5$ ,  $t = 12.5$ ,  $t = 120$  min vs. stress for  $n = 25$  specimens along (a) the parallel direction and (b) the perpendicular direction.

fibers (Fig. 4e) and, in each layer, the fibers were arranged into bundles (Fig. 4f) that were mainly oriented along the *in-vivo* loading direction (Fig. 4). We obtained consistent results with our previous study,<sup>37</sup> where we visualized *only* the cross-section of the USL/CL that was perpendicular to the main *in-vivo* loading direction. The fractions of fiber bundles with various straightness parameters and orientation angles (Figs. 5, 6 and 7) were quantified from the SEM images of the in-plane specimen section (section 1 in Fig. 1b) to aid the interpretation of the results of the creep experiments.

The measurement of the straightness parameters of the fiber bundles helped us shed some light on the relationship between the un-crimping process and the creep phenomenon. Hingorani *et al.*<sup>11</sup> speculated that fiber un-crimping was the creep mechanism in rabbit medial collateral ligaments. For most fiber bundles of the USL/CL complex, the straightness parameter varied between 0.82 and 0.94 (Fig. 6). This means that 6–18% of the fiber bundles could un-crimp before being stretched. This fiber bundle un-crimping likely contributed to creep. The result that the average fiber

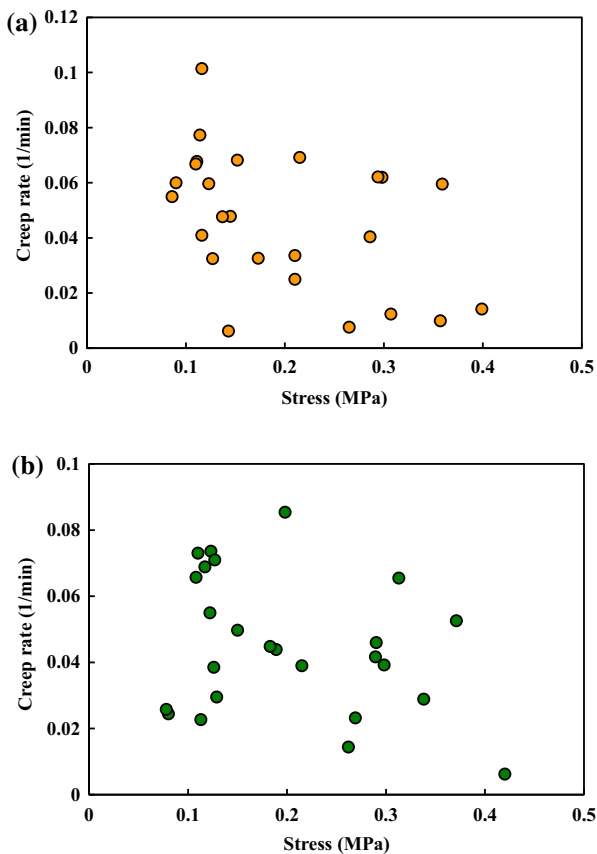


**FIGURE 12.** Creep rate vs. stress for  $n = 25$  specimens along (a) the parallel direction and (b) the perpendicular direction.

bundle straightness in the parallel direction was similar to the average fiber bundle straightness in the perpendicular direction may explain why creep was comparable in the two loading directions. We note that the straightness parameters of the USL/CL complex were, however, underestimated since the out-of-plane waviness of the fiber bundles was not captured in the two dimensional SEM images used for our analysis.

We determined a discrete distribution for the fractions of fiber bundles with different global orientation angles (Fig. 7). The global measurements of orientation indicated that the fibers were preferentially oriented along the parallel direction. This is to be expected since the collagen fibers must provide structural support to the ligaments mainly along their *in-vivo* loading direction. They also explain the previously observed elastic anisotropy of these ligaments<sup>3</sup>. Collagen fibers add structural strength to the USL/CL complex. The presence of a smaller fraction of collagen fiber bundles in the perpendicular direction may have determined the larger initial strain (Tables 1 and 2) and larger normalized strain during the entire creep test (Fig. 8) in this direction.

Over the past years, the mechanical properties of USLs have been characterized by quantifying their

deformation using engineering strain.<sup>19,29,41</sup> In this study, the USL/CL specimens underwent large deformation (strains up to 85% were recorded for one specimen in the perpendicular direction) during creep and, for this reason, the use of the engineering strain was deemed inappropriate. The Lagrangian strain was determined instead and was measured using the 3-D DIC method. This method accounted for the inhomogeneities in strain of the USL/CL complex that were neglected in our previous studies.<sup>3,37</sup> It must be noted that, inevitably, the safety pins used for gripping the specimens caused stress concentration. By using the 3-D DIC, we were able to compute the average strain during creep in the central region of the specimens located away from the safety pins, where the effects of stress concentration were absent. The 3-D DIC also excluded from the strain measurement possible artifacts due to the out-of-plane motion of the specimens during testing. Although the surface strain was accurately measured using the 3-D DIC, relative sliding of the thin layers that make the ligaments (Fig. 4e) may also have occurred, but was not captured. This speculation is based on the observed layer debonding that preceded complete failure during uniaxial tensile tests of the USL/CL.<sup>37</sup>

While negligible biaxial creep was reported over a 3-h period for the porcine mitral valve (mean radial stretch increased from 1.36 to 1.38 and mean circumferential stretch increased from 1.05 to 1.06 at an equibiaxial tension of 90 N/m)<sup>8</sup> and porcine aortic valve (mean radial stretch increased from 1.43 to 1.46 and mean circumferential stretch increased from 1.04 to 1.05 at an equibiaxial tension of 60 N/m),<sup>35</sup> noticeable biaxial creep was found over a 2-h period for the swine USL/CL complex. We recorded a mean normalized strain of 1.34 and 1.41 in the parallel and perpendicular directions, respectively, at constant equibiaxial loads of 2 N and a mean normalized strain of 1.20 and 1.33 in the parallel and perpendicular directions, respectively, at constant equibiaxial loads of 4 N (Fig. 8). The difference in the amount of biaxial creep between the heart valves and USL/CL complex is due to the difference in structure, composition, and physiological function between these tissues. Creep of the USL/CL complex is significant and surgeons should consider possible changes in the length of these ligaments in reconstructive surgeries for the utero-vaginal prolapse (e.g., uterosacral ligament fixation). Of course, mechanical experiments need to be conducted on human ligaments to determine whether a comparable increase in strain over time under constant equibiaxial loads can be observed. Nevertheless, given the similarities that exist between the human and swine USL and CL,<sup>37</sup> we believe that the data collected in this study indicate that creep may alter the supportive role of the USL and CL.

Equi-biaxial loads of 2 N and 4 N were used on the swine USL/CL complex to generate relatively low and high stresses (Tables 1 and 2). Higher normalized strains and creep rates were found at lower equi-biaxial loads in both loading directions (Figs. 4 and 9). The normalized strain, especially at 120 min (Fig. 10), decreased with increasing stress, as reported for rat and rabbit medial collateral ligaments.<sup>11,24</sup> Such decrease in creep with an increase in equi-biaxial load can be explained by the fact that, as the load increases, more fibers become straight and fewer fibers remain crimped.<sup>40</sup> Straight collagen fibers deform much less and support larger loads than crimped collagen fibers.<sup>25</sup> Thus, during creep tests, as the equi-biaxial load increases, the deformation of the tissue over time decreases. Of course, with this interpretation of our experimental data, we are assuming that the collagen fibers govern the tissue deformation, but there may be other tissue components and mechanisms that cause the observed differences in the normalized strain over time at equi-biaxial loads of 2 and 4 N. For example, it is possible that, as the equi-biaxial loads increase, more fluid exudes out of the tissue. The fluid in the tissue may allow the fibers to move and deform more easily. As the fluid decreases within the tissue at higher creep loads, the collagen fibers encounter more resistance to deformation. The creep rate was significantly higher at equi-biaxial loads of 2 N than at equi-biaxial loads of 4 N in the parallel direction. Again, this could be explained by the presence of more crimped fibers and thus subsequent larger strains at lower loads.

We compared the creep behavior of the swine USL/CL complex under the same equi-biaxial loads in the parallel and the perpendicular directions. The mean normalized strain at 120 min in the parallel direction was less than that in the perpendicular direction at both constant equi-biaxial loads of 2 and 4 N. However, no significant difference in the mean normalized strain at 120 min and creep rate were detected between the two loading directions at both equi-biaxial loads. It is possible that, during equi-biaxial loading, some of the collagen fibers reorient making the difference in mechanical properties along the two loading directions insignificant. The slight increase in creep in the perpendicular direction may be explained by fewer fibers and, thus, slightly more fluid movement in such direction.

The large variation reported for the normalized strain and creep rate data of the ligaments can be attributed to inter-animal and intra-animal variations (Figs. 8, 9, 10 and 11). Indeed, in this study, the specimens for mechanical testing were collected from four different sows. Moreover, even in one of our previous studies,<sup>37</sup> where the specimens were collected from a single sow, the uniaxial elastic properties of the USL/CL complex were found to be location-depen-

dent. In this study, the specimens had different cross-sectional areas and, for this reason, they experienced different stresses when subjected to the same equi-biaxial loads (2 or 4 N). The difference in stresses can also explain the large variation in the creep data presented in this study.

The experimental data presented here can guide the development of a structural constitutive equation for the USL/CL complex that accounts for collagen fiber orientation and crimping (see, for example, our structural modeling efforts for collagenous tissues<sup>6,33,34</sup>). More experiments are currently being conducted to reveal possible nonlinearities in the creep behavior of the USL/CL complex. The role of other micro-structural components on the mechanical response of this complex is also being investigated. Only by implementing high fidelity constitutive equations into robust finite element models, invaluable computational tools for testing surgical reconstruction methods for PFDs can be created.

## CONCLUSIONS

This study presents the first characterization of the collagen fiber organization and biaxial creep properties of the swine USL/CL complex. In this ligamentous complex, there were more collagen fiber bundles oriented along the main *in-vivo* loading direction (the parallel direction) than along the direction perpendicular to it (the perpendicular direction). In both loading directions, the USL and CL specimens deformed substantially over time under constant equi-biaxial load. Moreover, creep proceeded significantly faster in the parallel direction, but not significantly faster in the perpendicular direction, for ligaments subjected to lower equi-biaxial loads vs. higher equi-biaxial loads. Based on our micro-structural analysis, we speculated that fluid movement and fiber un-crimping determine the higher creep rate at lower loads in the parallel direction. The creep properties of the USL/CL complex should be taken into account in the development of new surgical reconstruction methods, including mesh materials, for the treatment of PFDs.

## ACKNOWLEDGMENTS

Funding was provided by NSF PECASE Grant No. 1150397.

## CONFLICT OF INTEREST

The authors have no conflict of interest.

## REFERENCES

- <sup>1</sup>Anssari-Benam, A., D. L. Bader, and H. R. Screen. Anisotropic time-dependant behaviour of the aortic valve. *J. Mech. Behav. Biomed. Mater.* 4:1603–1610, 2011.
- <sup>2</sup>Barber, M. D., A. G. Visco, A. C. Weidner, C. L. Amundsen, and R. C. Bump. Bilateral uterosacral ligament vaginal vault suspension with site-specific endopelvic fascia defect repair for treatment of pelvic organ prolapse. *Am. J. Obstet. Gynecol.* 183:1402–1411, 2000.
- <sup>3</sup>Becker, W. R., and R. De Vita. Biaxial mechanical properties of swine uterosacral and cardinal ligaments. *Bio-mech. Model. Mechanobiol.* 14:549–560, 2014.
- <sup>4</sup>Cosson, M., P. Debodinance, M. Boukerrou, M. P. Chauvet, P. Lobry, G. Crepin, and A. Ego. Mechanical properties of synthetic implants used in the repair of prolapse and urinary incontinence in women: which is the ideal material? *Int. Urogynecol. J.* 14:169–178, 2003.
- <sup>5</sup>Couri, B. M., A. T. Lenis, A. Borazjani, M. F. R. Paraiso, and M. S. Damaser. Animal models of female pelvic organ prolapse: lessons learned. *Exp. Rev. Obstet. Gynecol.* 7:249–260, 2012.
- <sup>6</sup>De Vita, R., and W. S. Slaughter. A structural constitutive model for the strain rate dependent behavior of anterior cruciate ligaments. *Int. J. Solids Struct.* 43:1561–1570, 2006.
- <sup>7</sup>DeLancey, J. O. Anatomic aspects of vaginal eversion after hysterectomy. *Am. J. Obstet. Gynecol.* 166:1717–1728, 1992.
- <sup>8</sup>Grashow, J. S., M. S. Sacks, J. Liao, and A. P. Yoganathan. Planar biaxial creep and stress relaxation of the mitral valve anterior leaflet. *Ann. Biomed. Eng.* 34:1509–1518, 2006.
- <sup>9</sup>Gruber, D. D., W. B. Warner, E. D. Lombardini, C. M. Zahn, and J. L. Buller. Anatomical and histological examination of the porcine vagina and supportive structures: in search of an ideal model for pelvic floor disorder evaluation and management. *Female Pelvic Med. Reconstr. Surg.* 17:110–114, 2011.
- <sup>10</sup>Hendrix, S. L., A. Clark, I. Nygaard, A. Aragaki, V. Barnabei, and A. McTiernan. Pelvic organ prolapse in the Women's Health Initiative: gravity and gravidity. *Am. J. Obstet. Gynecol.* 186:1160–1166, 2002.
- <sup>11</sup>Hingorani, R. V., P. P. Provenzano, R. S. Lakes, A. Escarcega, and R. Vanderby, Jr. Nonlinear viscoelasticity in rabbit medial collateral ligament. *Ann. Biomed. Eng.* 32:306–312, 2004.
- <sup>12</sup>Jenkins, V. Uterosacral ligament fixation for vaginal vault suspension in uterine and vaginal vault prolapse. *Am. J. Obstet. Gynecol.* 177:1337–1344, 1997.
- <sup>13</sup>Li, X., J. A. Kruger, J. W. Jor, V. Wong, H. P. Dietz, M. P. Nash, and P. M. Nielsen. Characterizing the ex vivo mechanical properties of synthetic polypropylene surgical mesh. *J. Mech. Behav. Biomed. Mater.* 37:48–55, 2014.
- <sup>14</sup>Lin, L. L., J. Y. Phelps, and C. Y. Liu. Laparoscopic vaginal vault suspension using uterosacral ligaments: a review of 133 cases. *J. Minim. Invasive. Gynecol.* 12:216–220, 2005.
- <sup>15</sup>Lionello, G., C. Sirieix, and M. Baleani. An effective procedure to create a speckle pattern on biological soft tissue for digital image correlation measurements. *J. Mech. Behav. Biomed. Mater.* 39:1–8, 2014.
- <sup>16</sup>Luo, J., T. M. Smith, J. A. Ashton-Miller, and J. O. DeLancey. In vivo properties of uterine suspensory tissue in pelvic organ prolapse. *J. Biomech. Eng.* 136:021016–021016-6, 2014.
- <sup>17</sup>MacLennan, A. H., A. W. Taylor, D. H. Wilson, and D. Wilson. The prevalence of pelvic floor disorders and their relationship to gender, age, parity and mode of delivery. *Br. J. Obstet. Gynecol.* 107:1460–1470, 2000.
- <sup>18</sup>Mangera, A., A. J. Bullock, C. R. Chapple, and S. MacNeil. Are biomechanical properties predictive of the success of prostheses used in stress urinary incontinence and pelvic organ prolapse? A systematic review. *Neurourol. Urodyn.* 31:13–21, 2012.
- <sup>19</sup>Martins, P., A. L. Silva-Filho, A. M. R. M. Fonseca, A. Santos, L. Santos, T. Mascarenhas, R. M. N. Jorge, and A. M. Ferreira. Strength of round and uterosacral ligaments: a biomechanical study. *Arch. Gynecol. Obstet.* 287:313–318, 2013.
- <sup>20</sup>Mauri, A., M. Perrini, A. E. Ehret, D. S. De Focatiis, and E. Mazza. Time-dependent mechanical behavior of human amnion: macroscopic and microscopic characterization. *Acta Biomater.* 11:314–323, 2015.
- <sup>21</sup>Moalli, P. A., N. S. Howden, J. L. Lowder, J. Navarro, K. M. Debes, S. D. Abramowitch, and S. L. Woo. A rat model to study the structural properties of the vagina and its supportive tissues. *Am. J. Obstet. Gynecol.* 192:80–88, 2005.
- <sup>22</sup>Nygaard, I., M. D. Barber, K. L. Burgio, K. Kenton, S. Meikle, and J. Schaffer. et-al. Prevalence of symptomatic pelvic floor disorders in US women. *JAMA* 300:1311–1316, 2008.
- <sup>23</sup>Olsen, A. L., V. J. Smith, J. O. Bergstrom, J. C. Colling, and A. L. Clark. Epidemiology of surgically managed pelvic organ prolapse and urinary incontinence. *Obstet. Gynecol.* 89:501–506, 1997.
- <sup>24</sup>Provenzano, P., R. Lakes, T. Keenan, and R. Vanderby, Jr. Nonlinear ligament viscoelasticity. *Ann. Biomed. Eng.* 29:908–914, 2001.
- <sup>25</sup>Provenzano, P. P., and R. Vanderby. Collagen fibril morphology and organization: implications for force transmission in ligament and tendon. *Matrix Biol.* 25:71–84, 2006.
- <sup>26</sup>Ramanah, R., M. B. Berger, B. M. Parratte, and J. O. DeLancey. Anatomy and histology of apical support: a literature review concerning cardinal and uterosacral ligaments. *Inter. Urogynecol. J.* 23:1483–1494, 2012.
- <sup>27</sup>Reay, N. H. J., J. C. Jones, L. J. Healy, S. King, S. Saini, and T. G. Shousha. Allen-Mersh. Pelvic connective tissue resilience decreases with vaginal delivery, menopause and uterine prolapse. *Br. J. Surg.* 90:466–472, 2003.
- <sup>28</sup>Rezakhaniha, R., A. Agianniotis, J. T. C. Schrauwen, A. Griffa, D. Sage, C. V. C. Bouten, F. N. van de Vosse, M. Unser, and N. Stergiopulos. Experimental investigation of collagen waviness and orientation in the arterial adventitia using confocal laser scanning microscopy. *Biomech. Model. Mechanobiol.* 11:461–473, 2012.
- <sup>29</sup>Rivault, G., C. Rubod, B. Dedet, M. Brieu, B. Gabriel, and M. Cosson. Comparative analysis of pelvic ligaments: a biomechanics study. *Int. Urogynecol. J.* 24:135–139, 2013.
- <sup>30</sup>Rubod, C., M. Boukerrou, M. Brieu, P. Dubois, and M. Cosson. Biomechanical properties of vaginal tissue. Part 1: new experimental protocol. *J. Urol.* 178:320–325, 2007.
- <sup>31</sup>Silva, W. A., R. N. Pauls, J. L. Segal, C. M. Rooney, S. D. Kleeman, and M. M. Karram. Uterosacral ligament vault suspension: five-year outcomes. *Obstet. Gynecol.* 108:255–263, 2006.
- <sup>32</sup>Smith, T. M., J. Luo, Y. Hsu, J. Ashton-Miller, J. O. DeLancey. A novel technique to measure in vivo uterine suspensory ligament stiffness. *Am. J. Obstet. Gynecol.* 209:484.e1–484.e7, 2013.

- <sup>33</sup>Sopakayang, R., and R. De Vita. A mathematical model for relaxation, creep, and strain stiffening in parallel-fibered collagenous tissues. *Med. Eng. Phys.* 33:1056–1063, 2011.
- <sup>34</sup>Sopakayang, R., R. De Vita, A. L. Kwansa, and J. W. Freeman. Elastic and viscoelastic properties of a type I collagen fiber. *J. Theor. Biol.* 293:197–205, 2012.
- <sup>35</sup>Stella, J. A., J. Liao, and M. S. Sacks. Time-dependent biaxial mechanical behavior of the aortic heart valve leaflet. *J. Biomech.* 40:3169–3177, 2007.
- <sup>36</sup>Subak, L. L., L. E. Waetjen, S. van den Eeden, D. H. Thom, E. Vittinghoff, and J. S. Brown. Cost of pelvic organ prolapse surgery in the United States. *Obstet. Gynecol.* 98:646–651, 2001.
- <sup>37</sup>Tan, T., F. M. Davis, D. D. Gruber, J. C. Massengill, J. L. Robertson, and R. De Vita. Histo-mechanical properties of the swine cardinal and uterosacral ligaments. *J. Mech. Behav. Biomed. Mater.* 42:129–137, 2015.
- <sup>38</sup>Thornton, G. M., A. Oliynyk, C. B. Frank, and N. G. Shrive. Ligament creep cannot be predicted from stress relaxation at low stress: a biomechanical study of the rabbit medial collateral ligament. *J. Orthop. Res.* 15:652–656, 1997.
- <sup>39</sup>Thornton, G. M., N. G. Shrive, and C. B. Frank. Altering ligament water content affects ligament pre-stress and creep behavior. *J. Orthop. Res.* 19:845–851, 2001.
- <sup>40</sup>Thornton, G. M., N. G. Shrive, and C. B. Frank. Ligament creep recruits fibres at low stresses and can lead to modulus-reducing fibre damage at higher creep stresses: a study in rabbit medial collateral ligament model. *J. Orthop. Res.* 20:967–974, 2002.
- <sup>41</sup>Vardy, M. D., T. R. Gardner, F. Cosman, R. J. Scotti, M. S. Mikhail, A. O. Preiss-Bloom, J. K. Williams, J. M. Cline, and R. Lindsay. The effects of hormone replacement on the biomechanical properties of the uterosacral and round ligaments in the monkey model. *Am. J. Obstet. Gynecol.* 192:1741–1751, 2005.
- <sup>42</sup>Wu, J. M., A. F. Hundley, R. G. Fulton, and E. R. Myers. Forecasting the prevalence of pelvic floor disorders in US women, to 2050. *Obstet. Gynecol.* 114(2009):1278–1283, 2010.